

Interband pairing as the origin of the sublattice dichotomy in monolayer FeSe/SrTiO₃

Zhipeng Xu,^{1,2} Shengshan Qin,^{3,*} Kun Jiang,^{1,2,†} and Jiangping Hu^{1,4,5,‡}

¹Beijing National Laboratory for Condensed Matter Physics and Institute of Physics, Chinese Academy of Sciences, Beijing 100190, China

²School of Physical Sciences, University of Chinese Academy of Sciences, Beijing 100190, China

³School of Physics, Beijing Institute of Technology, Beijing 100081, China

⁴Kavli Institute of Theoretical Sciences, University of Chinese Academy of Sciences, Beijing, 100190, China

⁵New Cornerstone Science Laboratory, Beijing, 100190, China

(Dated: November 13, 2025)

Sublattice dichotomy in monolayer FeSe/SrTiO₃, signaling the breaking of symmetries exchanging the two Fe sublattices, has recently been reported. We propose that interband pairing serves as the origin of this dichotomy, regardless of whether the symmetry is broken in the normal state or in the pairing state. If symmetry breaking occurs in the normal state, the Fermi surfaces are sublattice-polarized, and the intersubband d -wave pairing naturally acts as interband pairing, reproducing the observed dichotomy in the spectra. Alternatively, if symmetry breaking takes place in the pairing state, it manifests as the coexistence of intraband and interband pairing, with the constraint that interband pairings share the same sign while intraband pairings carry opposite signs. In both cases, interband pairing is indispensable, establishing it as a key ingredient for understanding superconductivity in monolayer FeSe/SrTiO₃.

I. INTRODUCTION

Iron-based superconductors have attracted sustained and widespread interest since their initial discovery^{1–10}, owing to their high critical temperatures, rich phase diagrams^{3,4,11–14}, and unconventional pairing mechanisms^{1,2,15–18}. Among these materials, a particularly striking development was the discovery of a record-high superconducting transition temperature (~ 65 K) in monolayer FeSe films grown on SrTiO₃ substrate^{19–26}. This system differs fundamentally from the usual iron pnictides. Angle-resolved photoemission spectroscopy (ARPES) measurements reveal that the hole-like bands near the Γ point are below the Fermi level, leaving only electron pockets at the Brillouin zone corner²⁷. The absence of the hole pockets invalidates the Fermi surface nesting scenario commonly invoked in the iron-based superconductors^{15,16}. Therefore, monolayer FeSe/SrTiO₃ has become a unique platform for exploring unconventional, interface-enhanced high- T_c superconductivity^{28–32}.

The monolayer FeSe consists of a single layer of Fe atoms arranged in a square lattice, sandwiched by two Se atomic layers positioned alternately above (Se^+) and below (Se^-) the Fe plane (see Fig. 1(a)). The alternating positioning of the Se atoms above and below the Fe plane doubles the size of the structural unit cell of the Fe square lattice, resulting in two Fe atoms per unit cell, named Fe_A and Fe_B . For the pristine monolayer FeSe, these two sublattices are equivalent to each other due to symmetries, such as inversion symmetry whose center locates at the middle of the Fe_A - Fe_B bond. In the material, however, the existence of substrate, electronic ordering, and many other issues may break the equivalence of the two sublattices.

Recently, sublattice dichotomy has been witnessed in the monolayer FeSe/SrTiO₃ in a scanning tunneling microscopy and spectroscopy (STM/STS) experiment³³. Distinct dual tunneling spectra within the pairing gap corresponding to the two Fe sublattices (schematically illustrated in Fig. 1(b)) are observed. Specifically, two superconducting gaps are identified, namely V_i and V_o . The coherence peak at $+V_i$ on Fe_A is lower

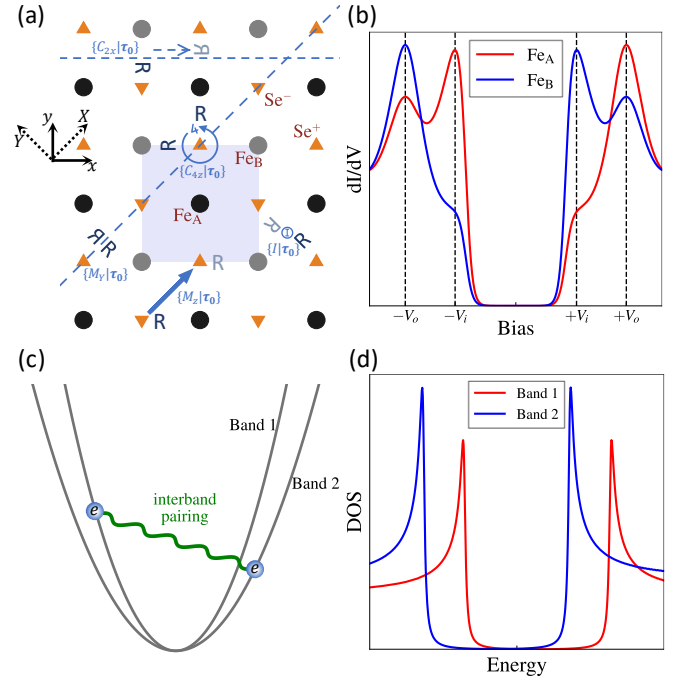


FIG. 1. (a) (Left) Coordinate systems used in this paper. (Right) Top view of monolayer FeSe. Fe atoms are depicted with solid circles in black and gray, corresponding to the two Fe sublattices. Se atoms above and below the Fe plane are represented by upward-pointing and downward-pointing filled triangles, respectively. Fe_A , Fe_B , Se^+ and Se^- are the notations for each type of atom. A single unit cell is indicated by the shaded square region. Symmetries exchanging the two Fe sublattices, $\{I|\tau_0\}$, $\{C_{4z}|\tau_0\}$, $\{M_y|\tau_0\}$, $\{M_z|\tau_0\}$, and $\{C_{2x}|\tau_0\}$ where $\tau_0 = (1/2, 1/2)$, are depicted in blue, with paired “R” symbols visualizing the symmetry action—each pair represents the original object and its image under the corresponding operation. The dark blue “R” is above the Fe plane, and the light blue one is below. The name of each symmetry is indicated nearby³⁴. (b) Schematic of the observed tunneling spectra on two sublattices. V_i and V_o are the inner and outer gaps. (c) Schematic of interband pairing. (d) Density of states (DOS) projected onto each band for a two-band superconductor with interband pairing³⁵.

than that on Fe_B , whereas the coherence peak at $-V_i$ on Fe_A is higher. Conversely, the intensity difference of the coherence peaks at $\pm V_o$ exhibits the opposite behavior. This intriguing phenomenon is reminiscent of interband pairing^{35–39} in multiband superconductors. The interband pairing describes Cooper pairs formed by electrons from bands with different masses, as illustrated in Fig. 1(c). Since the particle and hole sectors forming the Cooper pair are from the bands with distinct masses, such a subsystem intrinsically lacks particle–hole symmetry. Accordingly, the pairing between them necessarily produces particle–hole asymmetric spectra³⁵. Density of states (DOS) projected onto each band for a two-band superconductor with interband pairing are calculated in Ref. 35 and also presented here in Fig. 1(d). As shown, the coherence peaks of band 1 shift positively by half the energy difference between the two bands, while those of band 2 shift negatively by the same amount. Though the above analyses refer to the band-projected DOS in a two-band superconductor, the resulting spectra closely resemble the experimentally observed ones, i.e. the sublattice-projected DOS as displayed in Fig. 1(b) and (d). Therefore, we propose that interband pairing underlies the sublattice dichotomy.

This paper is organized as follows. Section II is devoted to the symmetry analysis, which identifies the symmetry requirement for realizing the sublattice dichotomy. Section III and IV discuss two cases: symmetry breaking in the normal state and in the pairing state, both of which emphasize the role of interband pairing. Section V is for summary and discussion.

II. SYMMETRY ANALYSIS

To figure out the origin of the sublattice dichotomy in monolayer $\text{FeSe}/\text{SrTiO}_3$, we start with a symmetry analysis. The pristine monolayer FeSe respects the space group $G = P4/nmm$, which is nonsymmorphic. Its quotient group G/\mathcal{T} with \mathcal{T} being the translation subgroup contains 16 symmetry operations as listed in Table. I, the point group part of which is isomorphic to the point group D_{4h} . The symmetry operations in G/\mathcal{T} can be classified into two categories; Half of the symmetry operations map the Fe_A sublattice to the Fe_B sublattice, and the others does not exchange the two Fe sublattices. We list the two categories of symmetry operations in Table. I, and schematically illustrate the symmetries exchanging the two Fe sublattices in Fig. 1(a). Here, we use the Seitz notation $\{g|\tau\}$ where g is a point group operation and τ is a translation, to describe the symmetry operations.

Due to the symmetries exchanging the two Fe sublattices, it is natural to expect exactly the same experimental observations at Fe_A and Fe_B in the monolayer $\text{FeSe}/\text{SrTiO}_3$. Conversely, the sublattice dichotomy observed in recent experiments unambiguously indicates that all the symmetry opera-

tions mapping Fe_A to Fe_B are broken. To realize such a condition, orders belonging to different irreducible representations must be present. Notably, in the Nambu basis the BdG Hamiltonian of a superconductor always belongs to the A_{1g} irreducible representation, if only one single pairing order is considered, regardless of the specific pairing symmetry. Hence, according to Table I the problem reduces to identifying a B_{2u} perturbation to the BdG Hamiltonian. Notice that the B_{2u} perturbations can be the superconducting pairing orders or the orders in the normal bands.

III. NORMAL STATE SYMMETRY BREAKING

We first consider the symmetries are broken in the normal state. We adopt the low-energy $k \cdot p$ model developed in Ref. 34, which resembles the electron pockets near the Brillouin zone corner, i.e. the M point, in the monolayer $\text{FeSe}/\text{SrTiO}_3$ ^{27,33}. The model respects the full symmetries of the space group $P4/nmm$, and takes the form $H_0 = \sum_{\mathbf{k},\sigma} \psi_{\sigma}^{\dagger}(\mathbf{k}) h_M(\mathbf{k}) \psi_{\sigma}(\mathbf{k})$ with

$$h_M(\mathbf{k}) = \begin{pmatrix} h_M^+(\mathbf{k}) & 0 \\ 0 & h_M^-(\mathbf{k}) \end{pmatrix}, \quad (1a)$$

where

$$h_M^{\pm}(\mathbf{k}) = \begin{pmatrix} \epsilon_1 + \frac{k^2}{2m_1} \pm a_1 k_x k_y & -iv_{\pm}(\mathbf{k}) \\ iv_{\pm}(\mathbf{k}) & \epsilon_3 + \frac{k^2}{2m_3} \pm a_3 k_x k_y \end{pmatrix}, \quad (1b)$$

and

$$v_{\pm}(\mathbf{k}) = v(\pm k_x + k_y) + p_1(\pm k_x^3 + k_y^3) + p_2 k_x k_y (k_x \pm k_y). \quad (1c)$$

The above Hamiltonian is written in the d -orbital basis

$$\psi_{\sigma}(\mathbf{k}) = \frac{1}{\sqrt{2}} \begin{pmatrix} d_{Xz,\sigma}^A(\mathbf{k}) - d_{Xz,\sigma}^B(\mathbf{k}) \\ d_{XY,\sigma}^A(\mathbf{k}) + d_{XY,\sigma}^B(\mathbf{k}) \\ d_{Yz,\sigma}^A(\mathbf{k}) + d_{Yz,\sigma}^B(\mathbf{k}) \\ d_{XY,\sigma}^A(\mathbf{k}) - d_{XY,\sigma}^B(\mathbf{k}) \end{pmatrix}, \quad (2)$$

where \mathbf{k} is measured from the M point, σ is the spin index, and A (B) stands for the the Fe_A (Fe_B) sublattice.

We use the above model to fit the experimentally reported Fermi surfaces of the monolayer $\text{FeSe}/\text{SrTiO}_3$ ³³, and derive the parameters as $\epsilon_1 = -95.00$, $\epsilon_3 = -60.00$, $\frac{1}{2m_1} = -2.40$, $\frac{1}{2m_3} = 20.58$, $a_1 = 38.06$, $a_3 = -48.56$, $v = 39.90$, $p_1 = -0.63$ and $p_2 = -1.87$, which are all in unit of meV. The corresponding Fermi surfaces showing the sublattice weight are presented in Fig. 2(a). As shown in the figure, on the Fermi surfaces the two sublattices are evenly mixed. This arises from the constraint imposed by the glide-mirror symmetry $\{M_z|\tau_0\}$ which exchanges the two Fe sublattices but leaves \mathbf{k} invariant.

Based on the low-energy effective model, we now consider

perturbations that break all the symmetries exchanging the

TABLE I. Character table of G/\mathcal{T} (isomorphic to D_{4h}), where τ_0 stands for the translation $(1/2, 1/2)$. The symmetry operations exchanging the two Fe sublattices are marked in blue.

	$\{E \mathbf{0}\}$	$\{2S_{4z} \mathbf{0}\}$	$\{C_{2z} \mathbf{0}\}$	$\{C_{2x/y} \mathbf{0}\}$	$\{M_{x/y} \mathbf{0}\}$	$\{I \tau_0\}$	$\{2C_{4z} \tau_0\}$	$\{M_{x/y} \tau_0\}$	$\{M_z \tau_0\}$	$\{C_{2x/y} \tau_0\}$
A_{1g}	1	1	1	1	1	1	1	1	1	1
A_{2g}	1	1	1	-1	-1	1	1	-1	1	-1
B_{1g}	1	-1	1	-1	1	1	-1	-1	1	1
B_{2g}	1	-1	1	1	-1	1	-1	1	1	-1
E_g	2	0	-2	0	0	2	0	0	-2	0
A_{1u}	1	-1	1	1	-1	-1	1	-1	-1	1
A_{2u}	1	-1	1	-1	1	-1	1	1	-1	-1
B_{1u}	1	1	1	-1	-1	-1	-1	1	-1	1
B_{2u}	1	1	1	1	1	-1	-1	-1	-1	-1
E_u	2	0	-2	0	0	-2	0	0	2	0

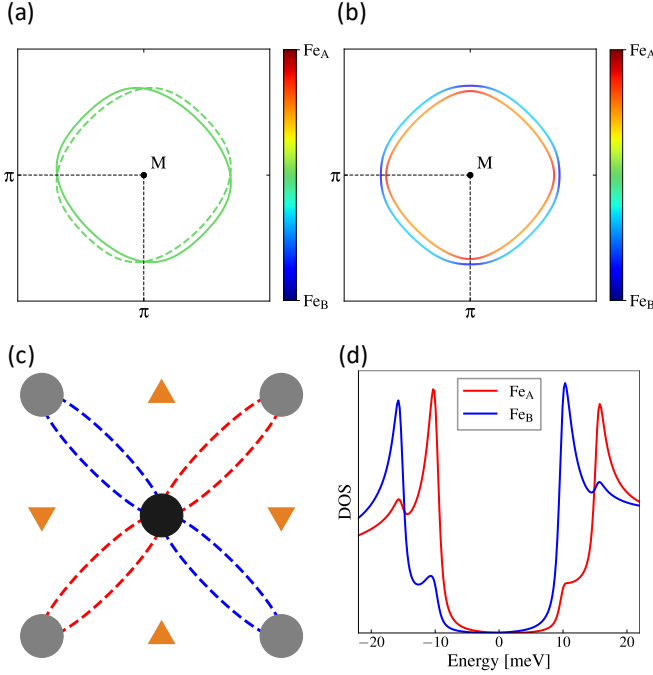


FIG. 2. (a) Fermi surfaces without symmetry-breaking terms. Parameters are taken as $\epsilon_1 = -95.00$, $\epsilon_3 = -60.00$, $\frac{1}{2m_1} = -2.40$, $\frac{1}{2m_3} = 20.58$, $a_1 = 38.06$, $a_3 = -48.56$, $v = 39.90$, $p_1 = -0.63$, $p_2 = -1.87$ in unit of meV to mimic the experimental Fermi surface results³³. (b) Fermi surfaces with symmetry-breaking terms. Parameters in $h'_M(\mathbf{k})$ are taken as $v_1 = v_2 = v_3 = v_4 = 1.00$ meV. The color in (a) and (b) represents the sublattice weight. (c) Schematic illustration of nodeless d -wave pairing in real space. The pairing is positive (red) in the X -direction and negative (blue) in the Y -direction. (d) Calculated DOS with the combination of normal state symmetry breaking Eq. (3) and nodeless d -wave pairing Eq. (4), where $\Delta_d = 12.20$ meV.

two Fe sublattices, i.e. the B_{2u} perturbations in the normal bands. Note that the B_{2u} perturbations in the normal state must also be the B_{2u} perturbations in the superconducting state. Under the basis in Eq. (2), up to the \mathbf{k}^2 order the perturbations

take the form

$$h'_M(\mathbf{k}) = \begin{pmatrix} 0 & 0 & v_3(k_x^2 - k_y^2) & -iv_4(k_x + k_y) \\ 0 & 0 & iv_4(-k_x + k_y) & v_1 + v_2 \mathbf{k}^2 \\ v_3(k_x^2 - k_y^2) & -iv_4(-k_x + k_y) & 0 & 0 \\ iv_4(k_x + k_y) & v_1 + v_2 \mathbf{k}^2 & 0 & 0 \end{pmatrix}. \quad (3)$$

Upon adding h'_M into h_M with $v_1 = v_2 = v_3 = v_4 = 1.00$ meV, the corresponding Fermi surfaces are shown in Fig. 2(b). Clearly, the sublattice weights are clearly redistributed; Specifically, the inner Fermi surface is predominantly contributed by Fe_A , while the outer one is mainly from Fe_B . The results suggest a correspondence between the sublattices and the bands. Thus, the intersublattice pairing effectively plays the role of the interband pairing, potentially giving rise to the features of Fig. 1(d). In the intersublattice pairing channel, the s -wave pairing gives nodal superconducting state. Considering the nodeless superconducting gap observed in the monolayer FeSe/SrTiO₃, we focus on the intersublattice d -wave pairing⁴⁰⁻⁴³, more specifically the d -wave pairing between the nearest-neighbor Fe_A and Fe_B sites. The d -wave pairing order changes sign under the S_4 symmetry as schematically illustrated in Fig. 2(c). As the Fermi surfaces are located around M which is S_4 invariant, superconducting nodes should have existed on the Fermi surfaces; However, due to the interband pairing nature of the intersublattice pairing, the d -wave pairing state is actually fully gapped.

The leading order of the nodeless d -wave pairing, expressed in form of $\psi^\dagger_\uparrow(\mathbf{k})\Delta(\mathbf{k})[\psi^\dagger_\downarrow(-\mathbf{k})]^T$, is given by

$$\Delta(\mathbf{k}) = \Delta_d \begin{pmatrix} 1 & 0 & 0 & 0 \\ 0 & 1 & 0 & 0 \\ 0 & 0 & -1 & 0 \\ 0 & 0 & 0 & -1 \end{pmatrix}. \quad (4)$$

Combining the normal-state perturbations in Eq.(3) and the nodeless d -wave pairing in Eq.(4), we calculate the DOS at Fe_A and Fe_B , and the results are presented in Fig. 2(d). As expected, the sublattice dichotomy of the superconducting coherence peaks is realized, due to the sublattice-polarized Fermi surfaces and the interband nature of the d -wave pairing.

Before ending this part, we note that incorporating the s_\pm pairing component, alongside the above d -wave pairing, does

not necessarily alter the sublattice dichotomy, provided that the magnitude of s_{\pm} component is not dominant.

IV. PAIRING STATE SYMMETRY BREAKING

The sublattice dichotomy in the monolayer FeSe/SrTiO₃ may also arise from the mix of the different pairing orders. To break the symmetries mapping Fe_A to Fe_B, according to Table. I one need to consider the following pairing combinations, $A_{1g} + B_{2u}$, $A_{2g} + B_{1u}$, $B_{1g} + A_{2u}$ and $B_{2g} + A_{1u}$. Here, we focus on the pairings belonging to the 1D irreducible representations. In fact, for each of the above pairing combinations, if we consider the even-parity (odd-parity) order separately the system is invariant under the crystalline symmetries, i.e. the BdG Hamiltonian belonging to the A_{1g} irreducible representation, and the odd-parity (even-parity) order serves as the B_{2u} perturbations in the sense of the BdG Hamiltonian.

For the iron-based superconductors, it has been revealed⁴⁴ that for the 1D irreducible representations the even-parity pairing orders correspond to intraband pairing, whereas the odd-parity orders correspond to interband pairing. To obtain the sublattice dichotomy in the monolayer FeSe/SrTiO₃, the coexistence of intraband and interband pairing serves as the starting point, and additional constraints on their relative phases must be imposed as we shall show in the following.

Before considering the monolayer FeSe/SrTiO₃, it is helpful to utilize a simple two-band model to develop some insights. We denote the band operators as $c_{1k\sigma}^{\dagger}$ and $c_{2k\sigma}^{\dagger}$, and assume simple dispersions $\gamma_1 k^2 - \mu$ and $\gamma_2 k^2 - \mu$ ($\gamma_1 > \gamma_2$) for the two bands. The BdG Hamiltonian under the basis $\Psi_k^{\dagger} = (c_{1k\uparrow}^{\dagger}, c_{2k\uparrow}^{\dagger}, c_{1,-k\downarrow}, c_{2,-k\downarrow})$ is

$$H_{\text{BdG}} = \begin{pmatrix} \gamma_1 k^2 - \mu & 0 & \Delta_{a1} & \Delta_{b1} \\ 0 & \gamma_2 k^2 - \mu & \Delta_{b2} & \Delta_{a2} \\ \Delta_{a1}^* & \Delta_{b2}^* & -\gamma_1 k^2 + \mu & 0 \\ \Delta_{b1}^* & \Delta_{a2}^* & 0 & -\gamma_2 k^2 + \mu \end{pmatrix}, \quad (5)$$

where $\Delta_{a1(2)}$ and $\Delta_{b1(2)}$ are the intraband and interband pairings, respectively. To determine the conditions under which the sublattice dichotomy emerges, we perform a perturbation analysis (details in the Supplemental Material) and find that the only pairing configuration yielding the sublattice dichotomy is $\Delta_{b1} = \Delta_{b2}$ and $\Delta_{a1} = -\Delta_{a2}$, i.e. the interband pairing having the same sign and the intraband pairing having opposite signs.

We examine the above criterion in the monolayer FeSe/SrTiO₃. Specifically, we consider the pairings $A_{1g} + B_{2u}$ as an example in the $k \cdot p$ model in Eq. (1a). The leading order of the B_{2u} pairing under the basis in Eq. (2) is

$$B_{2u} : \Delta(\mathbf{k}) = \Delta_{b2u} \begin{pmatrix} 0 & 0 & 0 & 0 \\ 0 & 0 & 0 & 1 \\ 0 & 0 & 0 & 0 \\ 0 & 1 & 0 & 0 \end{pmatrix}. \quad (6)$$

Based on the $k \cdot p$ in Eq. (1a), it can be found the B_{2u} pairing in Eq.(6) is actually the pure interband pairing which occurs in the d_{XY} orbital. Moreover, the B_{2u} pairing in Eq.(6) is even

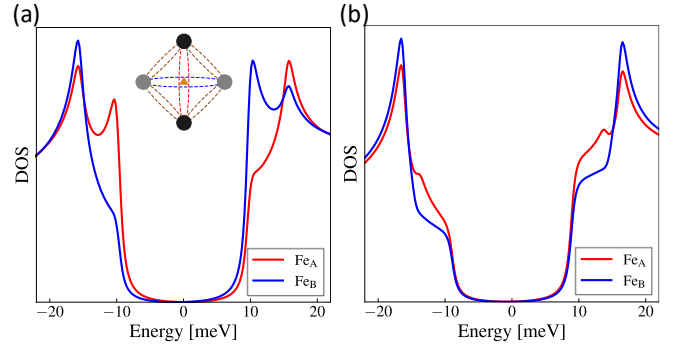


FIG. 3. Calculated DOSs with pairing combinations of (a) Eq. (6) with (7b), (b) (6) with (7a). Parameters are (a) $\Delta_{b2u} = 15$ meV, $\Delta_{a1g} = 10$ meV, (b) $\Delta_{b2u} = 18$ meV, $\Delta_{a1g} = -0.5$ meV. The inset in (a) is the schematic illustration of the pairing combination of Eq. (6) with (7b) in real space. The intrasublattice pairing is positive (red) on Fe_A-Fe_A bonds and negative (blue) on Fe_B-Fe_B bonds, while all intersublattice pairings share the same sign (brown).

with respect to the band indices, satisfying the criterion for the sublattice dichotomy. For the A_{1g} pairing, the two leading orders preserved up to \mathbf{k}^2 take the form

$$A_{1g} : \Delta(\mathbf{k}) = \Delta_{a1g} \begin{pmatrix} 1 & 0 & 0 & 0 \\ 0 & 1 & 0 & 0 \\ 0 & 0 & 1 & 0 \\ 0 & 0 & 0 & 1 \end{pmatrix}, \quad (7a)$$

$$A_{1g} : \Delta(\mathbf{k}) = \Delta_{a1g} \begin{pmatrix} k_x k_y & 0 & 0 & 0 \\ 0 & k_x k_y & 0 & 0 \\ 0 & 0 & -k_x k_y & 0 \\ 0 & 0 & 0 & -k_x k_y \end{pmatrix}. \quad (7b)$$

Based on the criterion developed in the above, only the A_{1g} pairing in Eq.(7b) which is odd with respect to the band indices satisfies the condition. We further simulate the superconducting DOSs with the B_{2u} pairing in Eq. (6) and the A_{1g} pairing in Eq.(7b), and present the results in Fig. 3(a). As expected, the sublattice dichotomy is observed at the Fe_A and Fe_B sites, consistent with the experiments. To compare, we also calculate the case with the B_{2u} pairing in Eq. (6) and the A_{1g} pairing in Eq.(7a); As shown in Fig. 3(b), no sublattice dichotomy appears.

In real space, for the above pairing combination responsible for the sublattice dichotomy, the B_{2u} order in Eq. (6) corresponds to the nearest-neighbour intrasublattice pairing which is S_4 invariant but have opposite signs in the Fe_A sublattice and Fe_B sublattice; While the A_{1g} order in Eq.(7b) describes the nearest-neighbour intersublattice pairing with a uniform pairing sign. We schematically illustrate the two pairing orders in the inset of Fig. 3(a). Such a pairing combination has been proposed in Ref. 44.

V. SUMMARY AND DISCUSSION

In summary, we have identified interband pairing as a key ingredient in understanding the sublattice dichotomy observed in the monolayer FeSe/SrTiO₃³³. Two possibilities are recognized for such symmetry-breaking. In the first case, symmetry-breaking is present in the normal state, leading to sublattice-polarized Fermi surfaces. The intersub-lattice d -wave pairing effectively acts as interband pairing, which can naturally reproduce the experimentally observed dichotomy in the spectra. However, we notice the nodeless d -wave pairing, is challenged by vortex-core STM/STS measurements⁴⁵, which report a CdGM spectrum inconsistent with d -wave-based theoretical predictions⁴⁶. This discrepancy calls further explorations. In the second case, symmetry breaking emerges at the superconducting level through a mixing of both intraband and interband pairing. Here, an ad-

ditional constraint is required: while the interband pairings must share the same sign, the intraband pairings must carry opposite signs.

Note added.—During the preparation of this manuscript, we became aware of Ref. 47, which also investigates the sublattice dichotomy in monolayer FeSe/SrTiO₃.

VI. ACKNOWLEDGMENTS

We acknowledge the support by the Ministry of Science and Technology (Grant No. 2022YFA1403900), the National Natural Science Foundation of China (Grant NSFC-12494594, No. NSFC-12174428, Grant No. NSFC-12304163), the New Cornerstone Investigator Program, the Chinese Academy of Sciences Project for Young Scientists in Basic Research (2022YSBR-048), and the Beijing Institute of Technology Research Fund Program for Young Scholars.

* qinshengshan@bit.edu.cn

† jiangkun@iphy.ac.cn

‡ jphu@iphy.ac.cn

- ¹ P J Hirschfeld, M M Korshunov, and I I Mazin, “Gap symmetry and structure of Fe-based superconductors,” *Reports on Progress in Physics* **74**, 124508 (2011).
- ² Andrey Chubukov, “Pairing mechanism in Fe-based superconductors,” *Annual Review of Condensed Matter Physics* **3**, 57–92 (2012).
- ³ Qimiao Si, Rong Yu, and Elihu Abrahams, “High-temperature superconductivity in iron pnictides and chalcogenides,” *Nature Reviews Materials* **1**, 16017 (2016).
- ⁴ Rafael M. Fernandes, Amalia I. Coldea, Hong Ding, Ian R. Fisher, P. J. Hirschfeld, and Gabriel Kotliar, “Iron pnictides and chalcogenides: a new paradigm for superconductivity,” *Nature* **601**, 35–44 (2022).
- ⁵ Yoichi Kamihara, Takumi Watanabe, Masahiro Hirano, and Hideo Hosono, “Iron-based layered superconductor La[O_{1-x}F_x]FeAs ($x = 0.05$ – 0.12) with $T_c = 26$ K,” *Journal of the American Chemical Society* **130**, 3296–3297 (2008).
- ⁶ Marianne Rotter, Marcus Tegel, and Dirk Johrendt, “Superconductivity at 38 K in the iron arsenide (Ba_{1-x}K_x)Fe₂As₂,” *Phys. Rev. Lett.* **101**, 107006 (2008).
- ⁷ Fong-Chi Hsu, Jiu-Yong Luo, Kuo-Wei Yeh, Ta-Kun Chen, Tzu-Wen Huang, Phillip M. Wu, Yong-Chi Lee, Yi-Lin Huang, Yan-Yi Chu, Der-Chung Yan, and Maw-Kuen Wu, “Superconductivity in the PbO-type structure α -FeSe,” *Proceedings of the National Academy of Sciences* **105**, 14262–14264 (2008).
- ⁸ Joshua H. Tapp, Zhongjia Tang, Bing Lv, Kalyan Sasmal, Bernd Lorenz, Paul C. W. Chu, and Arnold M. Guloy, “LiFeAs: An intrinsic FeAs-based superconductor with $T_c = 18$ K,” *Phys. Rev. B* **78**, 060505 (2008).
- ⁹ X.C. Wang, Q.Q. Liu, Y.X. Lv, W.B. Gao, L.X. Yang, R.C. Yu, F.Y. Li, and C.Q. Jin, “The superconductivity at 18 K in LiFeAs system,” *Solid State Communications* **148**, 538–540 (2008).
- ¹⁰ Jiangang Guo, Shifeng Jin, Gang Wang, Shunchong Wang, Kaixing Zhu, Tingting Zhou, Meng He, and Xiaolong Chen, “Superconductivity in the iron selenide K_xFe₂Se₂ ($0 \leq x \leq 1.0$),” *Phys. Rev. B* **82**, 180520 (2010).

- ¹¹ Rafael M. Fernandes, Andrey V. Chubukov, and Jörg Schmalian, “What drives nematic order in iron-based superconductors?” *Nature Physics* **10**, 97–104 (2014).
- ¹² Rafael M Fernandes and Andrey V Chubukov, “Low-energy microscopic models for iron-based superconductors: a review,” *Reports on Progress in Physics* **80**, 014503 (2016).
- ¹³ Pengcheng Dai, “Antiferromagnetic order and spin dynamics in iron-based superconductors,” *Rev. Mod. Phys.* **87**, 855–896 (2015).
- ¹⁴ Anna E Böhmer and Andreas Kreisel, “Nematicity, magnetism and superconductivity in FeSe,” *Journal of Physics: Condensed Matter* **30**, 023001 (2017).
- ¹⁵ I. I. Mazin, D. J. Singh, M. D. Johannes, and M. H. Du, “Unconventional superconductivity with a sign reversal in the order parameter of LaFeAsO_{1-x}F_x,” *Phys. Rev. Lett.* **101**, 057003 (2008).
- ¹⁶ Kazuhiko Kuroki, Seiichiro Onari, Ryotaro Arita, Hidetomo Usui, Yukio Tanaka, Hiroshi Kontani, and Hideo Aoki, “Unconventional pairing originating from the disconnected fermi surfaces of superconducting LaFeAsO_{1-x}F_x,” *Phys. Rev. Lett.* **101**, 087004 (2008).
- ¹⁷ Kangjun Seo, B. Andrei Bernevig, and Jiangping Hu, “Pairing symmetry in a two-orbital exchange coupling model of oxypnictides,” *Phys. Rev. Lett.* **101**, 206404 (2008).
- ¹⁸ Chen Fang, Yang-Le Wu, Ronny Thomale, B. Andrei Bernevig, and Jiangping Hu, “Robustness of s -wave pairing in electron-overdoped A_{1-y}Fe_{2-x}Se₂ (A=K,Cs),” *Phys. Rev. X* **1**, 011009 (2011).
- ¹⁹ Wang Qing-Yan, Li Zhi, Zhang Wen-Hao, Zhang Zuo-Cheng, Zhang Jin-Song, Li Wei, Ding Hao, Ou Yun-Bo, Deng Peng, Chang Kai, Wen Jing, Song Can-Li, He Ke, Jia Jin-Feng, Ji Shuai-Hua, Wang Ya-Yu, Wang Li-Li, Chen Xi, Ma Xu-Cun, and Xue Qi-Kun, “Interface-induced high-temperature superconductivity in single unit-cell FeSe films on SrTiO₃,” *Chin. Phys. Lett.* **29**, 037402–037402 (2012).
- ²⁰ Shaolong He, Junfeng He, Wenhao Zhang, Lin Zhao, Defa Liu, Xu Liu, Daixiang Mou, Yun-Bo Ou, Qing-Yan Wang, Zhi Li, Lili Wang, Yingying Peng, Yan Liu, Chaoyu Chen, Li Yu, Guodong Liu, Xiaoli Dong, Jun Zhang, Chuangtian Chen, Zuyan Xu, Xi Chen, Xucun Ma, Qikun Xue, and X.J. Zhou, “Phase diagram and electronic indication of high-temperature superconductivity

- at 65 K in single-layer FeSe films,” *Nature Materials* **12**, 605–610 (2013).
- 21 Shiyong Tan, Yan Zhang, Miao Xia, Zirong Ye, Fei Chen, Xin Xie, Rui Peng, Difei Xu, Qin Fan, Haichao Xu, Juan Jiang, Tong Zhang, Xinchun Lai, Tao Xiang, Jiangping Hu, Binping Xie, and Donglai Feng, “Interface-induced superconductivity and strain-dependent spin density waves in FeSe/SrTiO₃ thin films,” *Nature Materials* **12**, 634–640 (2013).
 - 22 J. J. Lee, F. T. Schmitt, R. G. Moore, S. Johnston, Y.-T. Cui, W. Li, M. Yi, Z. K. Liu, M. Hashimoto, Y. Zhang, D. H. Lu, T. P. Devereaux, D.-H. Lee, and Z.-X. Shen, “Interfacial mode coupling as the origin of the enhancement of T_c in FeSe films on SrTiO₃,” *Nature* **515**, 245–248 (2014).
 - 23 Zuocheng Zhang, Yi-Hua Wang, Qi Song, Chang Liu, Rui Peng, K.A. Moler, Donglai Feng, and Yayu Wang, “Onset of the meissner effect at 65K in FeSe thin film grown on Nb-doped SrTiO₃ substrate,” *Science Bulletin* **60**, 1301–1304 (2015).
 - 24 Jian-Feng Ge, Zhi-Long Liu, Canhua Liu, Chun-Lei Gao, Dong Qian, Qi-Kun Xue, Ying Liu, and Jin-Feng Jia, “Superconductivity above 100 K in single-layer FeSe films on doped SrTiO₃,” *Nature Materials* **14**, 285–289 (2015).
 - 25 Dennis Huang and Jennifer E. Hoffman, “Monolayer FeSe on SrTiO₃,” *Annual Review of Condensed Matter Physics* **8**, 311–336 (2017).
 - 26 Yu Xu, Hongtao Rong, Qingyan Wang, Dingsong Wu, Yong Hu, Yongqing Cai, Qiang Gao, Hongtao Yan, Cong Li, Chaohui Yin, Hao Chen, Jianwei Huang, Zhihai Zhu, Yuan Huang, Guodong Liu, Zuyan Xu, Lin Zhao, and X. J. Zhou, “Spectroscopic evidence of superconductivity pairing at 83 K in single-layer FeSe/SrTiO₃ films,” *Nature Communications* **12**, 2840 (2021).
 - 27 Defa Liu, Wenhao Zhang, Daixiang Mou, Junfeng He, Yun-Bo Ou, Qing-Yan Wang, Zhi Li, Lili Wang, Lin Zhao, Shaolong He, Yingying Peng, Xu Liu, Chaoyu Chen, Li Yu, Guodong Liu, Xiaoli Dong, Jun Zhang, Chuangtian Chen, Zuyan Xu, Jiangping Hu, Xi Chen, Xucun Ma, Qikun Xue, and X.J. Zhou, “Electronic origin of high-temperature superconductivity in single-layer FeSe superconductor,” *Nature Communications* **3**, 931 (2012).
 - 28 Q. Fan, W. H. Zhang, X. Liu, Y. J. Yan, M. Q. Ren, R. Peng, H. C. Xu, B. P. Xie, J. P. Hu, T. Zhang, and D. L. Feng, “Plain s -wave superconductivity in single-layer FeSe on SrTiO₃ probed by scanning tunnelling microscopy,” *Nature Physics* **11**, 946–952 (2015).
 - 29 Xiao Chen, S. Maiti, A. Linscheid, and P. J. Hirschfeld, “Electron pairing in the presence of incipient bands in iron-based superconductors,” *Phys. Rev. B* **92**, 224514 (2015).
 - 30 Dennis Huang, Tatiana A. Webb, Shiang Fang, Can-Li Song, Cui-Zu Chang, Jagadeesh S. Moodera, Efthimios Kaxiras, and Jennifer E. Hoffman, “Bounds on nanoscale nematicity in single-layer FeSe/SrTiO₃,” *Phys. Rev. B* **93**, 125129 (2016).
 - 31 A. Linscheid, S. Maiti, Y. Wang, S. Johnston, and P. J. Hirschfeld, “High T_c via spin fluctuations from incipient bands: Application to monolayers and intercalates of FeSe,” *Phys. Rev. Lett.* **117**, 077003 (2016).
 - 32 Y. Zhang, J. J. Lee, R. G. Moore, W. Li, M. Yi, M. Hashimoto, D. H. Lu, T. P. Devereaux, D.-H. Lee, and Z.-X. Shen, “Superconducting gap anisotropy in monolayer FeSe thin film,” *Phys. Rev. Lett.* **117**, 117001 (2016).
 - 33 Cui Ding, Zhipeng Xu, Xiaotong Jiao, Qiyin Hu, Wenxuan Zhao, Lexian Yang, Kun Jiang, Jin-Feng Jia, Lili Wang, Jiangping Hu, *et al.*, “Sublattice dichotomy in monolayer FeSe superconductor,” *arXiv:2406.15239* (2024).
 - 34 Vladimir Cvetkovic and Oskar Vafek, “Space group symmetry, spin-orbit coupling, and the low-energy effective hamiltonian for iron-based superconductors,” *Phys. Rev. B* **88**, 134510 (2013).
 - 35 Pengfei Li, Kun Jiang, and Jiangping Hu, “Paramagnetic contribution in superconductors with different-mass cooper pairs,” *Phys. Rev. B* **110**, 094517 (2024).
 - 36 Jiong Mei, Shengshan Qin, and Jiangping Hu, “Interband-pairing-boosted supercurrent diode effect in multiband superconductors,” *arXiv:2510.15788* (2025).
 - 37 Adriana Moreo, Maria Daghofer, Andrew Nicholson, and Elbio Dagotto, “Interband pairing in multiorbital systems,” *Phys. Rev. B* **80**, 104507 (2009).
 - 38 Jamil Tahir-Kheli, “Interband pairing theory of superconductivity,” *Phys. Rev. B* **58**, 12307–12322 (1998).
 - 39 O. V. Dolgov, E. P. Fetsiov, D. I. Khomskii, and K. Svozil, “Model of interband pairing in mixed valence and heavy fermion systems,” *Zeitschrift für Physik B Condensed Matter* **67**, 63–68 (1987).
 - 40 D. F. Agterberg, T. Shishidou, J. O’Halloran, P. M. R. Brydon, and M. Weinert, “Resilient nodeless d -wave superconductivity in monolayer FeSe,” *Phys. Rev. Lett.* **119**, 267001 (2017).
 - 41 T. A. Maier, S. Graser, P. J. Hirschfeld, and D. J. Scalapino, “ d -wave pairing from spin fluctuations in the K_xFe_{2-y}Se₂ superconductors,” *Phys. Rev. B* **83**, 100515 (2011).
 - 42 I. I. Mazin, “Symmetry analysis of possible superconducting states in K_xFe_ySe₂ superconductors,” *Phys. Rev. B* **84**, 024529 (2011).
 - 43 A. Kreisel, Y. Wang, T. A. Maier, P. J. Hirschfeld, and D. J. Scalapino, “Spin fluctuations and superconductivity in K_xFe_{2-y}Se₂,” *Phys. Rev. B* **88**, 094522 (2013).
 - 44 Jiangping Hu, “Iron-based superconductors as odd-parity superconductors,” *Phys. Rev. X* **3**, 031004 (2013).
 - 45 Chen Chen, Qin Liu, Wei-Cheng Bao, Yajun Yan, Qiang-Hua Wang, Tong Zhang, and Donglai Feng, “Observation of discrete conventional caroli–de gennes–matricon states in the vortex core of single-layer FeSe/SrTiO₃,” *Phys. Rev. Lett.* **124**, 097001 (2020).
 - 46 Ke Xiang, Da Wang, and Qianghua Wang, “Accidental zero modes in a multiorbital superconductor with spin-orbital coupling,” *Progress in Physics* **45**, 250–259 (2025).
 - 47 Mercè Roig, Kazi Ranjibul Islam, Basu Dev Oli, Huimin Zhang, PMR Brydon, Aline Ramires, Yue Yu, Michael Weinert, Lian Li, and Daniel F Agterberg, “Origin of sublattice particle-hole asymmetry in monolayer FeSe superconductors,” *arXiv:2511.02226* (2025).

Supplemental Material

VII. DETAILS OF THE PERTURBATION ANALYSIS

This section is devoted to the perturbation analysis of Hamiltonian Eq. (5) under different pairing configurations. Firstly, we consider the case: $\Delta_{b1} = \Delta_{b2} = \Delta_b$ and $\Delta_{a1} = -\Delta_{a2} = \Delta_a$. When $\Delta_a = 0$, the Hamiltonian is block-diagonal, with eigenvectors arranged column-wise as

$$\begin{pmatrix} 0 & -v_k & 0 & u_k \\ -v_k & 0 & u_k & 0 \\ u_k & 0 & v_k & 0 \\ 0 & u_k & 0 & v_k \end{pmatrix} \quad (S1)$$

corresponding to eigenvalues $(-E_k^+, -E_k^-, E_k^-, E_k^+)$. The eigenvalues are defined as $E_k^\pm = \mathcal{E}_k \pm \eta_k = \sqrt{\epsilon_k^2 + \Delta_b^2} \pm \eta_k$, where $\epsilon_k = \frac{\gamma_1 + \gamma_2}{2} k^2 - \mu$ and $\eta_k = \frac{\gamma_1 - \gamma_2}{2} k^2$. In the vicinity of the Fermi surface, these four energy levels give rise to the coherence peaks in Fig. 1(d). The BdG wavefunctions are defined as $u_k = \sqrt{\frac{1}{2}(1 + \frac{\epsilon_k}{\mathcal{E}_k})}$ and $v_k = \sqrt{\frac{1}{2}(1 - \frac{\epsilon_k}{\mathcal{E}_k})}$. Then we treat Δ_a as a perturbation. To first order, the eigenvectors become

$$\begin{pmatrix} -\frac{\Delta_a}{2E_k^+} u_k & -v_k & \frac{\Delta_a}{2E_k^-} v_k & u_k \\ -v_k & \frac{\Delta_a}{2E_k^-} u_k & u_k & -\frac{\Delta_a}{2E_k^+} v_k \\ u_k & \frac{\Delta_a}{2E_k^-} v_k & v_k & \frac{\Delta_a}{2E_k^+} u_k \\ -\frac{\Delta_a}{2E_k^+} v_k & u_k & -\frac{\Delta_a}{2E_k^-} u_k & v_k \end{pmatrix}. \quad (S2)$$

As shown in Fig. 2(a), the two Fe sublattices are evenly mixed on the Fermi surfaces in the pristine normal state. We thus assume that $c_{1k\sigma}^\dagger = \frac{1}{\sqrt{2}}(c_{Ak\sigma}^\dagger + c_{Bk\sigma}^\dagger)$, $c_{2k\sigma}^\dagger = \frac{1}{\sqrt{2}}(c_{Ak\sigma}^\dagger - c_{Bk\sigma}^\dagger)$. With this relation, we can compute the sublattice-projected DOS. Near the inner gap, the DOSs on sublattice Fe_A and Fe_B are

$$\begin{aligned} -E_k^- \left\{ \begin{aligned} \rho_A(\omega) &\sim \left| \frac{\Delta_a}{2E_k^-} u_k - v_k \right|^2 \delta(\omega + E_k^-), \\ \rho_B(\omega) &\sim \left| \frac{\Delta_a}{2E_k^-} u_k + v_k \right|^2 \delta(\omega + E_k^-); \end{aligned} \right. \\ +E_k^- \left\{ \begin{aligned} \rho_A(\omega) &\sim \left| \frac{\Delta_a}{2E_k^-} v_k + u_k \right|^2 \delta(\omega - E_k^-), \\ \rho_B(\omega) &\sim \left| \frac{\Delta_a}{2E_k^-} v_k - u_k \right|^2 \delta(\omega - E_k^-). \end{aligned} \right. \end{aligned} \quad (S3)$$

If we assume Δ_a is negative, it is clear that the coherence peak at $-E_k^-$ on Fe_A is higher than that on Fe_B whereas the coherence peak at $+E_k^-$ on Fe_A is lower, which is exactly the feature of Fig. 1(b). The situation for the outer gap, though not elaborated further here, likewise agrees with Fig. 1(b).

Next is the second case: $\Delta_{b1} = \Delta_{b2} = \Delta_b$ and $\Delta_{a1} = \Delta_{a2} = \Delta_a$. Since the expressions for the perturbed eigenvectors in this case are rather cumbersome, we neglect terms proportional to $u_k^2 - v_k^2$, which are negligible near the Fermi surface. Within this approximation, the result to first order is

$$\begin{pmatrix} -\frac{2u_k v_k^2 \Delta_a}{E_k^+ - E_k^-} & -v_k & -\frac{2u_k^2 v_k \Delta_a}{E_k^+ - E_k^-} & u_k \\ -v_k & \frac{2u_k v_k^2 \Delta_a}{E_k^+ - E_k^-} & u_k & \frac{2u_k^2 v_k \Delta_a}{E_k^+ - E_k^-} \\ u_k & -\frac{2u_k^2 v_k \Delta_a}{E_k^+ - E_k^-} & v_k & \frac{2u_k v_k^2 \Delta_a}{E_k^+ - E_k^-} \\ \frac{2u_k^2 v_k \Delta_a}{E_k^+ - E_k^-} & u_k & -\frac{2u_k v_k^2 \Delta_a}{E_k^+ - E_k^-} & v_k \end{pmatrix}. \quad (S4)$$

The sublattice-projected DOS is then

$$\begin{aligned} -E_k^- \left\{ \begin{aligned} \rho_A(\omega) &\sim \left| \frac{2u_k v_k^2 \Delta_a}{E_k^+ - E_k^-} - v_k \right|^2 \delta(\omega + E_k^-), \\ \rho_B(\omega) &\sim \left| \frac{2u_k v_k^2 \Delta_a}{E_k^+ - E_k^-} + v_k \right|^2 \delta(\omega + E_k^-); \end{aligned} \right. \\ +E_k^- \left\{ \begin{aligned} \rho_A(\omega) &\sim \left| \frac{2u_k^2 v_k \Delta_a}{E_k^+ - E_k^-} - u_k \right|^2 \delta(\omega - E_k^-), \\ \rho_B(\omega) &\sim \left| \frac{2u_k^2 v_k \Delta_a}{E_k^+ - E_k^-} + u_k \right|^2 \delta(\omega - E_k^-). \end{aligned} \right. \end{aligned} \quad (S5)$$

Unlike the previous case, where the sublattice contrast reversed between $-E_k^-$ and $+E_k^-$, the current result shows that sublattice Fe_A exhibits stronger coherence peaks at both energies, which is not the observed sublattice dichotomy.

Finally, we analyse the case: $\Delta_{b1} = -\Delta_{b2} = \Delta_b$ and no constraint on intraband pairing. Notably, in this case the BdG Hamiltonian Eq. (5) exhibits a symmetry

$$\begin{pmatrix} 0 & \sigma_z \\ -\sigma_z & 0 \end{pmatrix} H_{\text{BdG}}^* \begin{pmatrix} 0 & -\sigma_z \\ \sigma_z & 0 \end{pmatrix} = -H_{\text{BdG}}, \quad (\text{S6})$$

where σ_z is the Pauli matrix. If H_{BdG} has an eigenvector $(u_1, u_2, \dots, \dots)^T$ with energy E , then $(\dots, \dots, u_1^*, -u_2^*)^T$ is an eigenvector with energy $-E$. Owing to this symmetry, the DOS projected onto both sublattices is $(|u_1 + u_2|^2 + |u_1 - u_2|^2)\delta(\omega - E)$, indicating no distinction between the two Fe sublattices.

In conclusion, only the case with interband pairing of the same sign and intraband pairing of opposite signs can give rise to the sublattice dichotomy.